Fluid−Liquid and Fluid−Solid Transitions of Tetracontane in Propane

Alan Ka Chun Chan,[†] Pål V. Hemmingsen,[‡] and Maciej Radosz*,[†]

Department of Chemical Engineering and Macromolecular Studies Group, Louisiana State University, Baton Rouge, Louisiana 70803-7303, and Department of Chemical Engineering, Norwegian University of Science and Technology, N-7034 Trondheim, Norway

Fluid−liquid (FL) and fluid−solid (FS) transitions are measured for tetracontane in propane and calculated from an equation of state for tetracontane, tetratriacontane, and hexacontane. The calculated data are found to be in agreement with the experimental data. As expected, increasing the *n*-alkane concentration and increasing pressure are found to increase the FS transition temperature. Also, increasing the *n*-alkane molecular weight is found to increase the FL transition pressure.

Introduction

Long chain normal alkanes form miscible solutions with propane at elevated temperatures and pressures, and they are low-molar-mass prototypes of polyethylene solutions in propane. Understanding the phase behavior of such well-defined solutions is important. Experimental data on the phase behavior of binary mixtures of propane with long chain normal alkanes are scarce, especially on fluid−solid (FS) transitions at high pressures. Peters et al. (1992, 1993) measured such data for tetratriacontane ($C_{34}H_{70}$) and hexacontane ($C_{60}H_{122}$) in propane.

The goal of this work is to understand the fluid−liquid (FL) and fluid−solid transitions of binary systems containing a long chain normal alkane and propane. The approach is to measure both transitions with a light-scattering probe for tetracontane ($C_{40}H_{82}$) in propane and to use an equation of state to correlate these and other experimental data. The equation of state used in this work is the SAFT (Statistical Associating Fluid Theory) proposed by Huang and Radosz (1990).

Generic Phase Diagrams

Figure 1 shows a generic $P-T$ phase diagram of a propane (C_3) + normal alkane (C_n) system, which is of type V in the classification of van Konynenburg and Scott (1980). When the difference in size between the two pure components increases, hence the degree of molecular-size asymmetry increases, a liquid−liquid−vapor (LLV) region develops, and the critical locus becomes discontinuous, as shown in Figure 1. One branch of the critical locus connects the critical point of the less volatile component (C_n) and a lower critical end point (LCEP). The other branch of the critical locus connects the critical point of the more volatile component (C_3) and an upper critical end point (UCEP). The three-phase transition line (LLV) connects the two critical end points. Peters et al. (1989) report the LCEP and UCEP values for different propane + *n*-alkane systems.

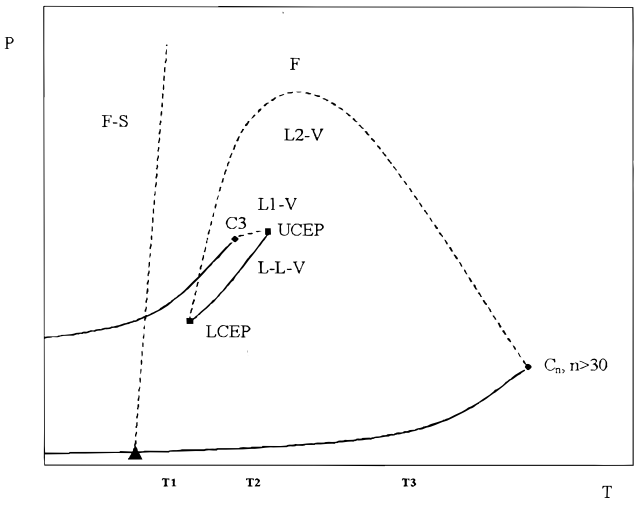

Figure 1. Generic pressure−temperature phase diagram for a type V propane (C_3) + normal alkane (C_n) system.

An FS transition curve is also shown in Figure 1. For normal alkanes, the FS transition curve shifts to higher temperatures as the carbon number increases. For large carbon numbers, the FS transition curve can overlap the LCEP, for example, for propane + hexacontane, as suggested by Peters et al. (1993).

Generic $P-X$ phase diagrams at three different temperatures corresponding to T_1, T_2, and T_3 in Figure 1 are shown in Figure 2. As expected on the basis of Figure 1, the two-phase regions at T_2 are separated by a three-phase line. In this study, all the experimental data are taken at temperatures higher than the LLV temperature T_2.

Experimental Section

The measurements are carried out in a high-pressure cell coupled with a light-scattering probe. The cell has a sapphire window and a borescope for visual observation of the phase transitions. The pressure is measured with a 0−500 bar dial gauge to within ±0.5 bar, and the temperature is measured with a three-wire class A RTD probe to within ±0.1 K. A simplified schematic of the unit is shown in Figure 3. A detailed description of the apparatus, the

* Corresponding author. E-mail: radosz@che.lsu.edu. Telephone: 225-388-1750. Fax: 225-388-1476.
[†] Louisiana State University.
[‡] Norwegian University of Science and Technology.

10.1021/je980306+ CCC: $19.00
Published on Web 02/18/2000

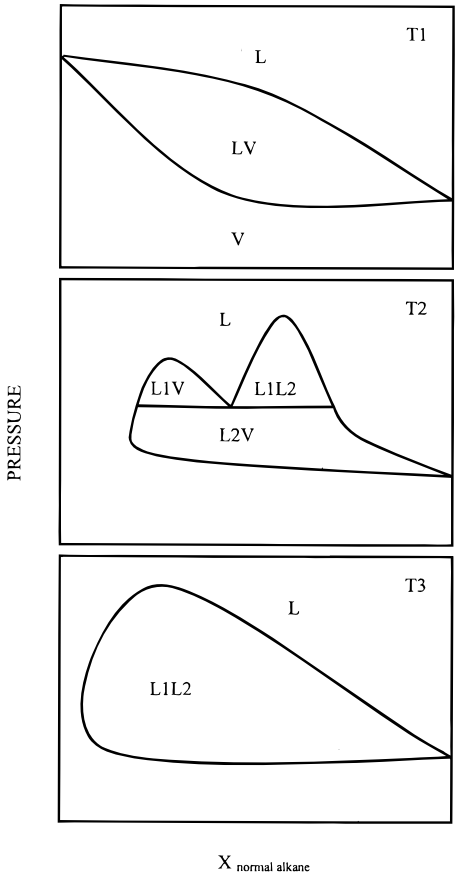

Figure 2. Generic pressure−concentration phase diagram for a type V propane (C_3) + normal alkane (C_n) system at different temperatures.

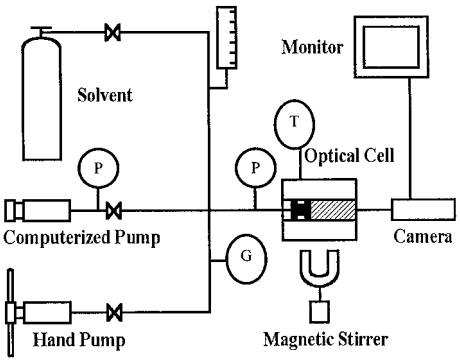

Figure 3. Simplified schematic diagram of the apparatus (G = Heise dial gauge, P = pressure transducer, T = temperature probe).

precision, and the experimental procedure is given by Chan et al. (2000).

Fluid−Liquid Transition Measurement. A known amount of solute and solvent is loaded in the cell. The amount of each component is determined with an analytical balance (Mettler-Toledo, Inc., Model PM 1200) to within ±0.002 g. The solution is then compressed, heated, and mixed to become homogeneous. The pressure is controlled with a floating piston; the pressurizing fluid is usually one of the components, for example, propane in this work. After equilibration, pressure is decreased at a constant rate while the intensity of transmitted light is recorded as a function of pressure at constant temperature. As the FL transition is reached, the solution turns cloudy, which can be observed visually. The onset of the solution turbidity at the FL pressure, also known as the binodal point, sharply decreases the transmitted-light intensity. Figure 4 shows a sample of a plot of the transmitted-light intensity as a function of pressure, where the cloud-point pressure is 69 bar.

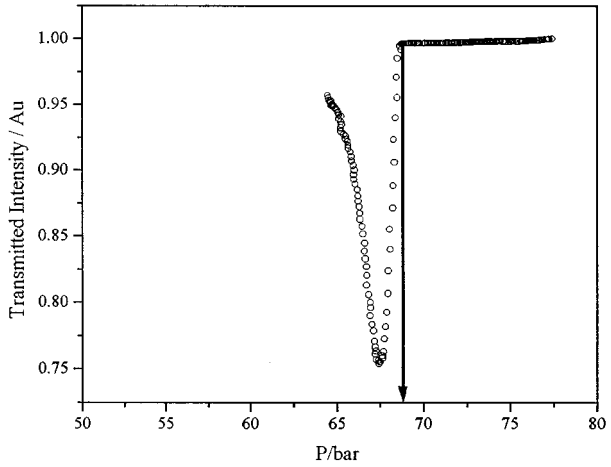

Figure 4. Plot of transmitted intensity as a function of pressure for the determination of the fluid−liquid phase transition pressure. C_{40} mass fraction = 0.079, t = 110 °C.

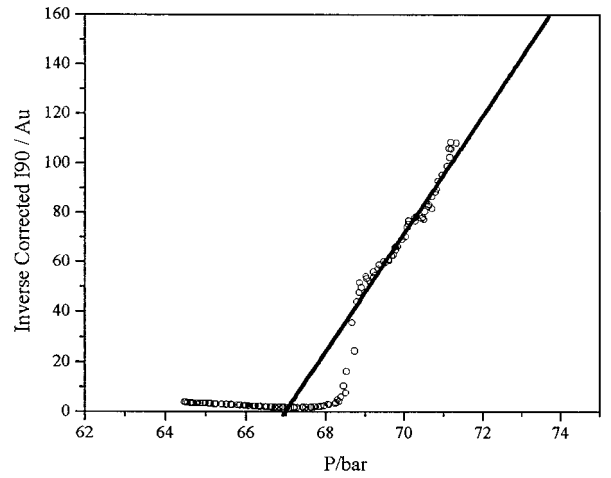

Figure 5. Plot of inverse corrected intensity at a 90° scattering angle as a function of pressure for the determination of spinodal pressure. C_{40} mass fraction = 0.079, t = 110 °C.

Spinodal Measurement. The intensity of scattered light is recorded as a function of pressure at the same time. The spinodal pressure is determined by the Debye−Scholte extrapolation procedure, as given by Kiepen and Borchard (1988) and Wells et al. (1993). The details of the approximations and corrections for this approach are given by Chan et al. (2000). In brief, according to the equation given by Wells et al. (1993),

$$(I_{90}^{\mathrm{corr}})^{-1} = C(P - P_s)_{\mathrm{isothermal}} \qquad (1)$$

where P_s is the spinodal pressure and C is a constant at fixed temperature and solution composition. The reciprocal of the corrected 90° scattered-light intensity $(I_{90}^{\mathrm{corr}})^{-1}$ is plotted as a function of pressure at constant temperature. The spinodal pressure is then obtained by extrapolating the $(I_{90}^{\mathrm{corr}})^{-1}$ to zero. A plot of $(I_{90}^{\mathrm{corr}})^{-1}$ as a function of pressure is shown in Figure 5 for propane + tetracontane at 110 °C; the spinodal pressure in this case is about 67 bar.

Fluid−Solid Transition Measurement. The solution is first equilibrated in the one-phase region. Temperature

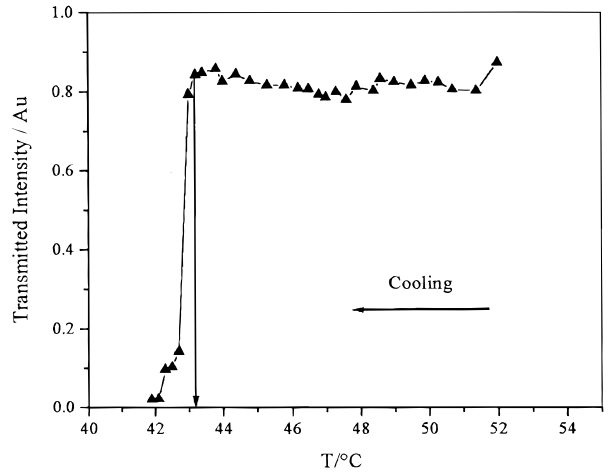

Figure 6. Plot of transmitted intensity as a function of temperature for determination of the fluid−solid transition temperature upon cooling (43.1 °C in this case). C_{40} mass fraction = 0.185, P = 400 bar.

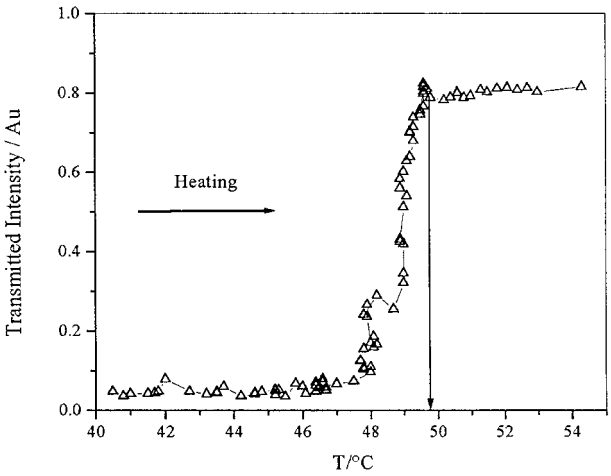

Figure 7. Plot of transmitted intensity as a function of temperature for determination of the fluid−solid transition temperature upon heating (49.6 °C in this case). C_{40} mass fraction = 0.185, P = 400 bar.

is then gradually decreased at constant pressure. The cooling rate close to the FS temperature is at or below 0.5 K/min. The transmitted-light intensity is recorded as a function of temperature. As the transition occurs, the signal decreases rapidly, as shown in Figure 6. The temperature corresponding to the drop in the signal intensity is recorded as the FS temperature upon cooling. This temperature is found to be very close to that observed visually, which corresponds to the onset of solid precipitation.

Another approach to measure the FS transition is to observe the disappearance of solids in the solution upon heating, as suggested, for example, by Hong et al. (1993). This is done by cooling the solution below the FS temperature and then slowly heating the stirred solution until the last traces of solid disappear. The heating rate is controlled at no more than 1 K/min. In this study, the transmitted-light intensity is also recorded as a function of temperature; a sample is shown in Figure 7. The temperature representing the onset of the flat portion of the transmitted-light intensity curve is taken as the FS temperature upon heating. The FS temperature obtained this way is also found to agree with that observed visually, which corresponds to the disappearance of solids.

The FS temperature measured upon heating is systematically higher than that upon cooling, as is shown in

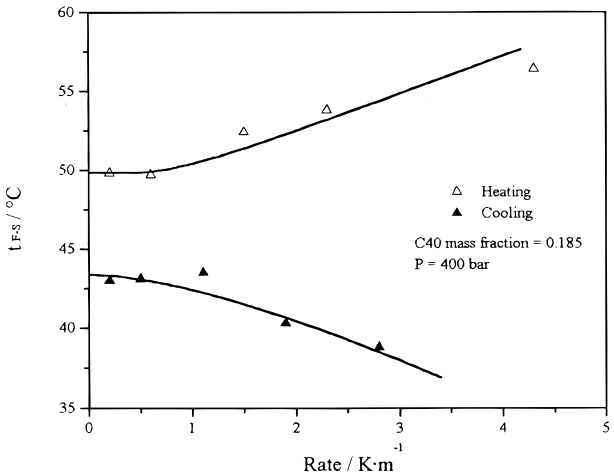

Figure 8. Effect of the heating and cooling rate on the fluid−solid transition temperature.

Figure 8. This is consistent with the previously published data, for example, by Kohn et al. (1976), who studied the ethane + *n*-octane, + *n*-decane, and + *n*-dodecane systems. They found that the degree of subcooling varied from 1 to 2 °C for *n*-octane and *n*-decane and from 3 to 7 °C for *n*-dodecane. The reason for the discrepancy between the heating-induced and cooling-induced FS temperatures is the subcooling effect that inhibits the nucleation of crystals in solution. The superheating effect, which inhibits the dissolution of crystals, is usually less significant, and hence, the heating-induced FS temperature is usually accepted as being closer to a true equilibrium FS temperature. Moreover, the measured FS temperature depends on the heating and cooling rate, except in the low-rate region, as is also shown in Figure 8. Therefore, the heating and cooling rates for this study are kept below 1 K/min to minimize the inaccuracy of the transition measurement due to kinetic effects.

Materials

The materials used in this study are tetracontane (98%), obtained from Aldrich Chemical Co., and propane (C.P., 99.0% minimum purity), obtained from Matheson Gas Products, Inc. They are used without further purification.

Equation of State

The equation of state used in this work to calculate the FS and FL transitions is an applied version of the statistical associating fluid theory (SAFT) proposed by Huang and Radosz (1990). SAFT molecules are homobonded chains, chains that are composed of identical segments connected with identical bonds. The SAFT residual Helmholtz energy a^{res} has segment, a^{seg}, chain, a^{chain}, and association, a^{assoc}, contributions, as follows:

$$a^{res} = a^{seg} + a^{chain} + a^{assoc} \quad (2)$$

The segment term is further divided into the hard-sphere, a^{hs}, and dispersion, a^{disp}, terms.

$$a^{seg} = a^{hs} + a^{disp} \quad (3)$$

Since the molecules used in this study do not exhibit any specific interactions, the association contribution term in eq 2 is set equal to zero.

Three parameters are used to characterize the pure components: the segment number, m, the temperature-independent segment volume of the segment, v^{oo}, and the

Table 1. Pure-Component SAFT Parameters

component	molar mass / g·mol^{-1}	m	$v^{\circ\circ}$ / cm^3·mol seg^{-1}	u°/k / K
propane, C_3H_8[a]	44.097	2.696	13.457	193.03
tetratriacontane, $C_{34}H_{70}$[b]	478.94	23.045	11.985	209.96
tetracontane, $C_{40}H_{82}$[b]	563.10	26.971	11.963	210.00
tetracontane, $C_{40}H_{82}$[c]	563.10	18.251	22.207	336.58
hexacontane, $C_{60}H_{122}$[b]	843.64	40.057	11.920	210.00

[a] The SAFT parameters are from Huang and Radosz (1990). [b] The SAFT parameters are calculated from an empirical equation for *n*-alkanes in Huang and Radosz (1990). [c] The SAFT parameters are estimated by fitting *PVT* data from Doolittle (1964) for liquid volume in the fluid−solid equilibria calculation.

temperature-independent dispersion energy of interaction between segments, u°/k. For small components, for example propane, the parameters are determined by fitting the pure-component vapor pressure and liquid density. For large components, for example tetracontane, the parameters are obtained from an empirical correlation based on the component molecular weight, as given by Huang and Radosz (1990). The parameter values used in this work are given in Table 1.

SAFT is extended to mixtures using the van der Waals one-fluid theory (vdW1) mixing rules as follows:

$$\frac{u}{kT} = \frac{\sum_i \sum_j x_i x_j m_i m_j \left[\frac{u_{ij}}{kT}\right] (v^\circ)_{ij}}{\sum_i \sum_j x_i x_j m_i m_j (v^\circ)_{ij}} \tag{4}$$

where

$$(v^\circ)_{ij} = \left[\frac{1}{2}[(v^\circ)_i^{1/3} + (v^\circ)_j^{1/3}]\right]^3 \tag{5}$$

$$u_{ij} = (1 - k_{ij})(u_{ii} u_{jj})^{1/2} \tag{6}$$

$$m = \sum_i \sum_j x_i x_j m_{ij} \tag{7}$$

$$m_{ij} = \frac{1}{2}(m_i + m_j) \tag{8}$$

where x_i is the mole fraction of component i, m is the segment number, v° is the temperature-dependent segment volume, u/k is the temperature-dependent dispersion energy of interaction between segments. k_{ij} is an adjustable binary parameter characterizing the interactions between component i and j; the k_{ij} values used for this study is 0.01.

In this study, a SAFT-based FS-E model developed by Pan and Radosz (1998) is used to calculate the fluid-solid equilibria. In brief, the fugacity ratio of pure *n*-alkane is given by

$$\ln\left(\frac{f_{02}^{L}}{f_{02}^{S}}\right) = -\ln\left(\frac{\phi_2^L x_2^L}{\phi^\circ}\right) = \frac{\Delta H_m}{RT_m}\left(\frac{T_m}{T} - 1\right) + \frac{\Delta H_{ss}}{RT_{ss}}\left(\frac{T_{ss}}{T} - 1\right) + \frac{\Delta C_p}{R}\left(1 - \frac{T_{ss}}{T}\right) - \frac{\Delta C_p}{R} \ln \frac{T}{T_{ss}} + \frac{\Delta C_p'}{R}\left(\frac{T_{ss} - T_m}{T}\right) - \frac{\Delta C_p'}{R} \ln \frac{T_{ss}}{T_m} + \frac{1}{RT}\int_{P^{sat}}^{P} (v^L - v^S)\, dP \tag{9}$$

where f is the fugacity and ϕ is the fugacity coefficient. ΔH_m and T_m are the enthalpy and temperature of fusion; ΔH_{ss} and T_{ss} are the enthalpy and temperature of the solid−solid transition. ΔC_p is the heat capacity difference between the liquid and solid phase, and $\Delta C_p'$ is the heat capacity difference between the liquid and the second solid phase; P^{sat} is the vapor pressure of the solute at its melting temperature, and v is the molar volume of the solute. The subscript 02 means pure solute, and the subscript 2 means solute in the solution. ϕ° is the fugacity coefficient of the pure subcooled liquid solute at constant temperature and pressure. Both fugacity coefficients in eq 9 are calculated from SAFT.

Table 2. Melting Properties and Solid−Solid Transition of Solutes

	T_m[a] / K	ΔH_m[b] / kJ/mol	T_{ss}[b] / K	ΔH_{ss}[b] / kJ/mol
tetratriacontane	346.3	78	343.1	41
tetracontane	354.5	92	351.3	49
hexacontane	371.9	138	368.7	73

[a] TRC a-1030, aa-ref-1920. [b] The values of the solid−solid transition and the melting properties are extrapolated from those data from Haulait-Pirson et al. (1987) and Chang et al. (1983).

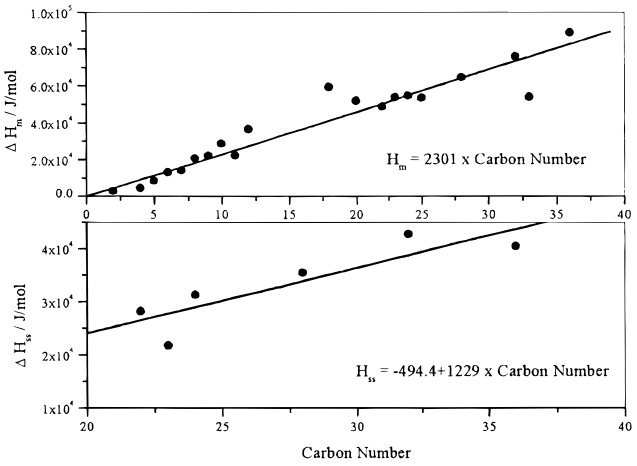

Figure 9. Correlation of the enthalpy of fusion, ΔH_m, the enthalpy of the solid−solid transition, ΔH_{ss}, and the carbon number of normal alkanes.

All four heat capacity terms have the same order of magnitude but opposite signs and tend to cancel each other; these four terms, therefore, are set equal to zero. Moreover, two assumptions are made for eq 9. First, the molar volume of the solid, v^S, is assumed to be constant, while the molar volume of the liquid, v^L, is a function of pressure. Second, the very low saturated pressure of the solute is set to zero. As a result, eq 9 becomes

$$-\ln\left(\frac{\phi_2^L x_2^L}{\phi^\circ}\right) = \frac{\Delta H_m}{RT_m}\left(\frac{T_m}{T} - 1\right) + \frac{\Delta H_{ss}}{RT_{ss}}\left(\frac{T_{ss}}{T} - 1\right) + \frac{1}{RT}\left(\int_0^P v^L\, dP - v^S P\right) \tag{10}$$

When the fluid−solid transition temperature is higher than the solid−solid transition temperature, the solid−solid transition terms should not be included in eq 10. This will be the case for very high solute concentration when the fluid−solid transition is close to the melting point of the solute.

The solid−solid and melting properties of the solutes are given in Table 2. For the heat of fusion and solid−solid transition, the values are obtained from linear regression of the data given by Haulait-Pirson et al. (1987) and Chang

Table 3. Experimental Phase Transitions for Propane (1) + Tetracontane (2) at Various Tetracontane Mass Fractions m_2

m_2	t/°C	P/bar	transition type[a]
0.014	160.3	92	FL
0.014	150.1	86	FL
0.014	140.4	79	FL
0.014	130.3	72	FL
0.014	120.3	62	FL
0.014	110.6	52	FL
0.014	100.5	43	FL
0.014	39.8	1207	FS
0.014	34.6	804	FS
0.014	29.6	407	FS
0.014	27.3	152	FS
0.031	119.8	69	FL
0.031	110.4	59	FL
0.031	110.4	47	spinodal
0.031	101.2	47	FL
0.065	130.3	86	FL
0.065	122.0	79	FL
0.065	110.5	64	FL
0.065	100.8	54	FL
0.065	95.4	46	FL
0.065	47.5	1200	FS
0.065	40.6	701	FS
0.065	39.1	501	FS
0.065	37.4	301	FS
0.065	36.9	100	FS
0.065	54.5	1200	FS*
0.065	46.9	701	FS*
0.065	45.1	501	FS*
0.065	43.6	301	FS*
0.068	120.2	79	FL
0.068	110.2	66	FL
0.068	110.2	60	spinodal
0.068	101.3	54	FL
0.079	120.2	80	FL
0.079	110.5	69	FL
0.079	110.5	67	spinodal
0.079	101.3	59	FL
0.104	159.8	110	FL
0.104	149.6	102	FL
0.104	140.0	93	FL
0.104	130.0	83	FL
0.104	120.1	74	FL
0.104	110.3	64	FL
0.104	101.3	54	FL
0.104	48.1	1208	FS
0.104	44.4	805	FS
0.104	39.6	408	FS
0.104	38.4	150	FS
0.150	119.7	81	FL
0.150	110.1	70	FL
0.150	101.3	60	FL
0.185	160.2	110	FL
0.185	150.3	101	FL
0.185	140.1	92	FL
0.185	130.3	81	FL
0.185	120.3	70	FL
0.185	110.1	59	FL
0.185	100.6	45	FL
0.185	53.9	1207	FS
0.185	49.9	805	FS
0.185	44.0	408	FS
0.185	42.5	152	FS
0.185	57.8	1207	FS*
0.185	53.2	805	FS*
0.185	46.9	408	FS*
0.185	48.6	152	FS*
0.250	120.0	86	FL
0.250	110.3	76	FL
0.250	100.5	65	FL

[a] Key: FL = fluid−liquid transition; FS = fluid−solid transition (cooling); FS* = fluid−solid transition (heating).

et al. (1983), as shown in Figure 9. Moreover, to calculate the pressure integral in eq 10 more accurately, we specialize the pure-component SAFT parameters by fitting *PVT* data for tetracontane reported by Doolittle (1964). These new *PVT*-derived parameters, given in Table 1, are only used for calculating the liquid molar volume in the pressure integral in eq 10; the usual correlation-derived parameters are used for calculating all the other properties.

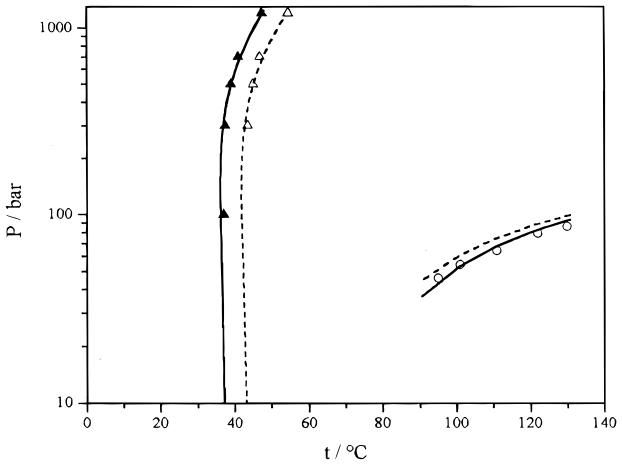

Figure 10. Pressure−temperature diagram of C_{40} + propane at fixed concentration. C_{40} mass fraction = 0.065; ρ_s = 0.95 g·cm^{-3}; open circles, FL; open triangles, FS upon heating; filled triangles, FS upon cooling; solid curve, SAFT with k_{ij} = 0.00; dashed curve, SAFT with k_{ij} = 0.01.

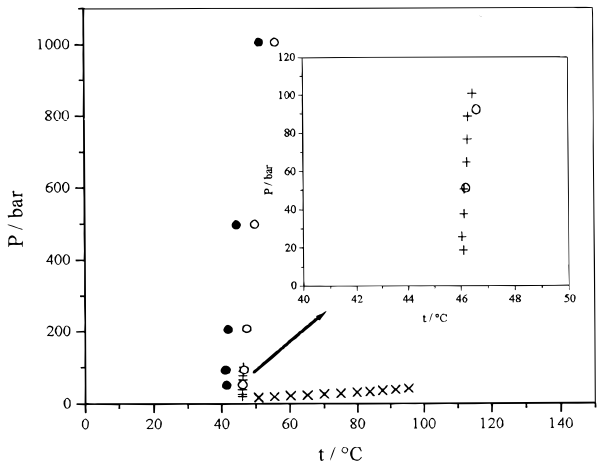

Figure 11. Pressure−temperature diagram of C_{34} + propane at fixed concentration. C_{34} mass fraction = 0.25; open circles, FS upon heating from this work; filled circles, FS upon cooling from this work; +, FS upon heating from Peters et al. (1992); ×, LV from Peters et al. (1992).

Results and Discussion

A summary of the experimental data for C_{40} + propane measured in this study is given in Table 3. Figure 10 shows a $P-T$ diagram of tetracontane + propane on the basis of the experimental data taken in this work. The FS transition curve shows a positive slope at high pressures, which means that the FS temperature increases with increasing pressure. Both the FS and FL transitions are calculated from SAFT twice; once with k_{ij} = 0 and once with k_{ij} = 0.01. The calculated results obtained with k_{ij} = 0 seem to represent better the FS temperature upon cooling, whereas the calculated results obtained with k_{ij} = 0.01 seem to represent better the FS temperature upon heating. Since we are more interested in modeling the FS temperature upon cooling, because it is relevant to pipeline fouling, our further analysis will not include the FS temperature upon heating. Let us emphasize that these k_{ij}'s, therefore, may

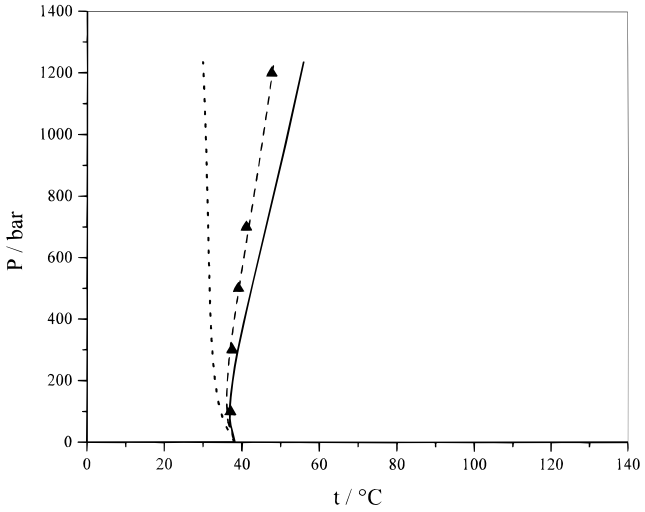

Figure 12. Pressure−temperature diagram of C_{40} + propane at fixed concentration. C_{40} mass fraction = 0.065; filled triangles, experimental FS upon cooling. SAFT calculation with $k_{ij} = 0.00$: solid curve, $\rho_s = 1.00$ g·cm^{-3}; dashed curve, $\rho_s = 0.95$ g·cm^{-3}; dotted curve, $\rho_s = 0.85$ g·cm^{-3}.

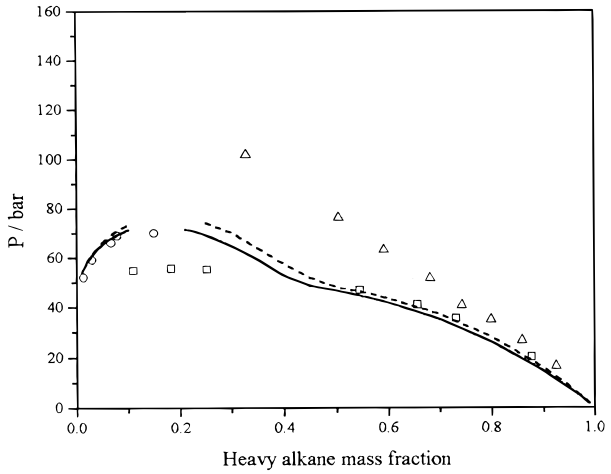

Figure 13. Fluid−liquid equilibria: Pressure−concentration diagram at 110 °C. Open triangles, propane + C_{60} by Peters et al. (1993); open circles, propane + C_{40} from this work; open squares, propane + C_{34} by Peters et al. (1992); solid curve, propane + C_{40} by SAFT with $k_{ij} = 0.00$; dashed curve, propane + C_{40} by SAFT with $k_{ij} = 0.01$.

represent a nonequilibrium FS transition (upon cooling) that is shifted relative to the equilibrium FS transition (upon heating).

To test our experimental approach, we reproduce the data for tetratriacontane + propane reported by Peters et al. (1992) at low pressures. Our data are found to be consistent with those reported by Peters et al. (1992), as shown in Figure 11. In addition, we measured both heating- and cooling-induced FS temperatures at higher pressures for tetratriacontane + propane. The FS temperature curve is found to have a positive slope, and the degree of subcooling is found to be about 5 °C.

The FS transition curve is found to be sensitive to the solid density ρ_s. Figure 12 shows an example where the solid density is changed from 0.85 g·cm^{-3} (∼density of subcooled liquid tetracontane) to 1.00 g·cm^{-3} (∼density of crystalline polymer). As a result, the FS transition is shifted to higher temperatures, especially at higher pressures. Since the density of crystalline tetracontane is not available, it is set equal to 0.95 g·cm^{-3}, which matches our

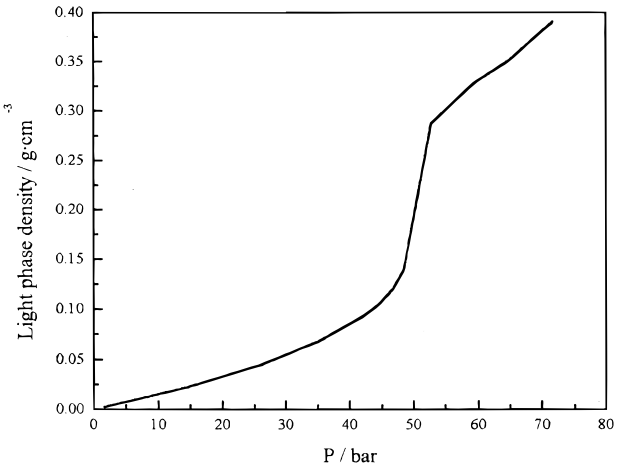

Figure 14. Equilibrium vapor-phase density at 110 °C as a function of pressure for C_3 + C_{40} calculated from SAFT ($k_{ij} = 0.00$).

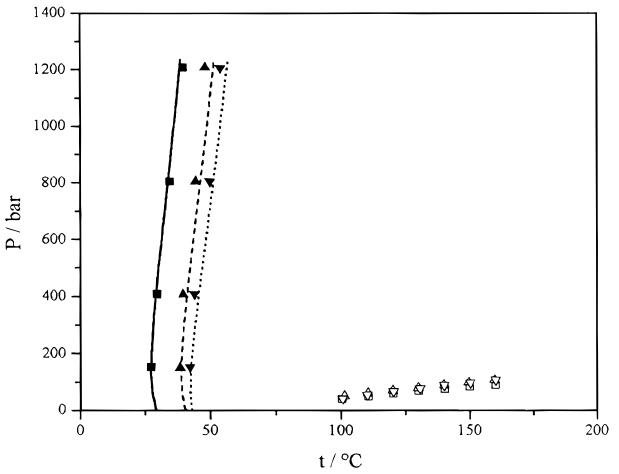

Figure 15. Pressure−temperature diagram of C_{40} + propane: concentration effect on fluid−solid equilibria upon cooling. The calculated curves are from SAFT with $k_{ij} = 0.00$ and $\rho_s = 0.95$ g·cm^{-3}. Filled squares and solid curve, mass fraction = 0.014; filled triangles and dashed curve, mass fraction = 0.104; filled circle and dotted curve, mass fraction = 0.185. Open symbols are fluid−liquid data.

data. This density is used to calculate the molar volume of the solid needed in eq 10.

Figure 13 shows a $P-X$ diagram of the FL transitions for tetratriacontane +, tetracontane +, and hexacontane + propane, where the points represent experimental data. The curves represent data calculated with the SAFT with $k_{ij} = 0$ and 0.01 for tetracontane + propane only. There is a change of the isotherm slopes around the heavy-alkane weight fraction of 0.4−0.5. Such a change of the slope has also been observed for other propane systems by Radosz (1987). This effect is due to a significant increase in the light-phase density upon increasing pressure, as is shown in Figure 14 at 110 °C for tetracontane + propane. A steep increase in the light-phase density is observed around 50 bar.

The effect of *n*-alkane concentration on the FS transition curve is shown in Figure 15 for tetracontane + propane at different tetracontane mass fractions. An increase in the tetracontane concentration increases the FS temperature. The calculated FS curves are in good agreement with the experimental data.

The effect of pressure on the FS transition is shown in Figure 16. An increase in pressure increases the FS

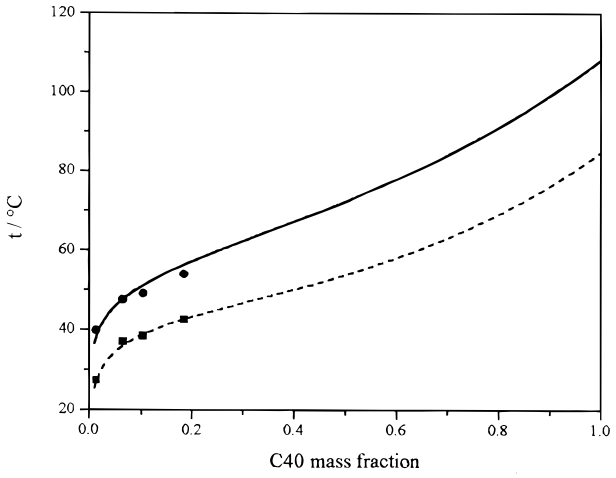

Figure 16. Temperature−concentration diagram of C_{40} + propane: pressure effect on fluid−solid equilibria upon cooling. The calculated curves are from SAFT with $k_{ij} = 0.00$ and $\rho_s = 0.95$ g·cm^{-3}. Filled circles and solid curve, $P = 1200$ bar; filled square and dashed curve, $P = 150$ bar.

temperature. Also shown in Figure 16 is the increase in the crystallization point of tetracontane with increasing pressure. SAFT captures both trends.

Conclusions

The fluid−liquid and fluid−solid equilibria for tetracontane measured in this work in sub- and supercritical propane are correlated and predicted using the SAFT equation of state. As expected, increasing the *n*-alkane concentration and increasing the pressure are found to increase the FS transition temperature. Also, increasing the *n*-alkane molecular weight is found to increase the FL transition pressure. SAFT predictions are found to be in reasonable agreement with the experimental data for both fluid−liquid and fluid−solid transitions.

Literature Cited

Chan, A. K. C.; Russo, P. S.; Radosz, M. Fluid-Liquid Equilibria in Poly(ethylene-*co*-hexene-1) + Propane: A Light-Scattering Probe of Cloud-Point Pressure, Spinodal Pressure, and Critical Polymer Concentration. *Fluid Phase Equilib.* **2000**, to be published.

Chang, S. S.; Maurey, J. R.; Pummer, W. J. Solubilities of Two *n*-Alkanes in Various Solvents. *J. Chem. Eng. Data* **1983**, *28*, 187−189.

Doolittle, A. K. Specific Volumes of *n*-Alkanes. *J. Chem. Eng. Data* **1964**, *9*, 275−279.

Haulait-Pirson, M.; Huys, G.; Vanstraelen, E. New Predictive Equation for the Solubility of Solid *n*-Alkanes in Organic Solvents. *Ind. Eng. Chem. Res.* **1987**, *26*, 447−452.

Hong, S. P.; Green, K. A.; Luks, K. D. Phase equilibria of the mixtures methane + *n*-hexane + n-hexatricontane, methane + toluene + naphthalene, and methane + *n*-hexane + naphthalene. *Fluid Phase Equilib.* **1993**, *87*, 255−272.

Huang, S. H.; Radosz, M. Equation of State for Small, Large, Polydisperse, and Associating Molecules. *Ind. Eng. Chem. Res.* **1990**, *29*, 2284−2294.

Kiepen, F.; Borchard, W. Pressure-Plused-Induced Critical Scattering of Oligostyrene in *n*-Pentane. *Macromolecules* **1988**, *21*, 1784−1790.

Kohn, J. P.; Luks, K. D.; Liu, P. H. Three-Phase Solid−Liquid−Vapor Equilibria of Binary *N*-Alkane Systems (Ethane−*n*-Octane, Ethane−*n*-Decane, Ethane−*n*-Dodecane). *J. Chem. Eng. Data* **1976**, *21*, 360−362.

van Konynenburg, P. H.; Scott, R. L. Critical Lines and Phase Equilibria in Binary van der Waals Mixtures. *Philos. Trans. R. Soc. (London)* **1980**, *298*, 495−540.

Pan, C.; Radosz, M. Copolymer SAFT Modeling of Phase Behavior in Hydrocarbon-Chain Solutions: Alkane Oligomers, Polyethylene, Poly(ethylene-*co*-olefin-1), Polystyrene, and Poly(ethylene-*co*-styrene). *Ind. Eng. Chem. Res.* **1998**, *37*, 3169−3179.

Peters, C. J.; van der Kooi, H. J.; de Roo, J. L.; de Swaan Arons, J.; Gallagher, J. S.; Sengers, J. M. H. L. The Search for Tricriticality in Binary Mixtures of Near-critical Propane and Normal Paraffins. *Fluid Phase Equilib.* **1989**, *51*, 339−351.

Peters, C. J.; de Roo, J. L.; de Swaan Arons, J. Measurements and Calculations of Phase Equilibria in Binary Mixtures of Propane + Tetratricontane. *Fluid Phase Equilib.* **1992**, *72*, 251−266.

Peters, C. J.; de Roos, J. L.; de Swaan Arons, J. Phase Equilibria in Binary Mixtures of Propane and Hexacontane. *Fluid Phase Equilib.* **1993**, *85*, 301−312.

Radosz, M. Multiphase Behavior of Supercritical Fluid Systems: Oil Solutions in Light Hydrocarbon Solvents. *Ind. Eng. Chem. Res.* **1987**, *26*, 2134−2139.

TRC Thermodynamic Tables−Hydrocarbons, a-1030, **1956**; aa-ref-1920 **1961**; Thermodynamics Research Center: Texas A&M University System, College Station, TX, extant 1996.

Wells, P. A.; de Loos, T. W.; Kleintjens, L. A. Pressure Pulsed Induced Critical Scattering: Spinodal and Binodal Curves for the System Polystyrene + Methylcyclohexane. *Fluid Phase Equilib.* **1993**, *83*, 383−390.

Received for review December 8, 1998. Accepted December 13, 1999.

JE980306+